Materials Today Communications 50 (2026) 114375

Contents lists available at ScienceDirect

Materials Today Communications

journal homepage: www.elsevier.com/locate/mtcomm

Light-driven composite films with photomechanical salicylideneaniline crystals aligned in UV-curing resins for soft actuators

Shodai Hasebe [a,*,1], Takashi Ueno [b,1], Yuki Hagiwara [b,2], Taiki Goto [c], Jérémy Odent [d], Jean-Marie Raquez [d], Hideko Koshima [e,*], Toru Asahi [a,b,c,e]

[a] Comprehensive Research Organization, Waseda University, 2-2 Wakamatsu-cho, Shinjuku-ku, Tokyo 162-8480, Japan
[b] Graduate School of Advanced Science and Engineering, Waseda University, 3-4-1 Okubo, Shinjuku-ku, Tokyo 169-8555, Japan
[c] School of Advanced Science and Engineering, Waseda University, 3-4-1 Okubo, Shinjuku-ku, Tokyo 169-8555, Japan
[d] Laboratory of Polymeric and Composite Materials (LPCM), Center of Innovation and Research in Materials and Polymers (CIRMAP), University of Mons (UMONS), Place Du Parc 20, Mons 7000, Belgium
[e] Research Organization for Nano & Life Innovation, Waseda University, 513, Waseda Tsurumakicho, Shinjuku-ku, Tokyo 162-0041, Japan

ARTICLE INFO

Keywords:
Crystal–polymer composite films
UV-curable resin
Salicylideneaniline
Photomechanical crystals

ABSTRACT

Photomechanical crystals—a subclass of crystalline materials that exhibit macroscopic deformation under light illumination—have applications in light-driven actuators and soft robots. However, they are associated with several drawbacks, such as size limitations to the millimeter scale and poor processability, which hinder their practical applications. Although several composite materials in which photomechanical crystals are aligned in a polymer membrane have been developed, the size of the photomechanical crystals has not been optimized, nor have the mechanical properties of the composite materials been investigated in detail. Here we demonstrated centimeter-scale, light-responsive, crystal–polymer composite films consisting of salicylideneaniline microcrystals and ultraviolet (UV)-curing resins. Desired-size single microcrystals were prepared by using the reprecipitation method or sublimation. Upon UV irradiation to the films, they bent away from the light source through photoisomerization or the photothermal effect, demonstrating their ability as an energy converter from light to kinetic work. The composite films exhibited distinct bending reversibility depending on the polymer matrix, originating from the polymer's different mechanical properties. Our composites provide insight into the development of centimeter-scale photomechanical materials with high processability, and, ultimately, light-fueled actuators and soft robots.

1. Introduction

The conversion of energy into mechanical motion is of vital importance in many engineering and technological fields. Various actuators—devices that convert an input energy source into mechanical energy—are indispensable in modern applications. Recently, stimuli-responsive soft materials have gained significant attention as a promising source for soft actuators [1]. By combining these soft actuators, soft robots can be fabricated, which offer distinct functional advantages over conventional robots made from rigid materials. Among external stimuli, light is a particularly attractive stimulus because it enables remote stimulation of target materials without direct contact, providing high spatial and temporal resolution [2,3]. Furthermore, light is advantageous because its properties, including wavelength, intensity, and polarization, can be precisely optimized for specific needs [2,3]. Since the beginning of the 21st century, various light-responsive (photomechanical) polymers incorporating azobenzene as a chromophore have been reported [1,3–6]. Upon irradiation with ultraviolet (UV) light, these polymers exhibit macroscopic deformation such as bending due to the strain generated by the *trans–cis* photoisomerization of the azobenzene moieties [1,3–6].

In addition to polymers, several organic molecular crystals [7]—including diarylethene [8,9], azobenzene [10,11], anthracene [12,13], and salicylideneaniline [14–16]—also exhibit light-induced shape

* Corresponding authors.
E-mail addresses: jenepaletemps@suou.waseda.jp (S. Hasebe), h.koshima@kurenai.waseda.jp (H. Koshima).
[1] S.H. and T.U. contributed equally.
[2] Present address: Research Institute for Microbial Diseases, The University of Osaka, 3-1 Yamadaoka, Suita, Osaka 565-0871, Japan.

https://doi.org/10.1016/j.mtcomm.2025.114375
Received 1 October 2025; Received in revised form 11 November 2025; Accepted 21 November 2025
Available online 26 November 2025

deformation. These photomechanical crystals show superior actuator performance compared to photomechanical polymers, including faster response times and higher power density [17]. Despite these advantages, photomechanical crystals face several drawbacks, such as size limitations (up to millimeter scales) and poor processability, which have hindered their practical application in macroscopic actuators and soft robots. Composite materials are expected to display novel properties not possessed by their individual constituent materials. For instance, several antimicrobial composites have been reported through the incorporation of antibacterial silver nanoparticles or nanowires into a polymer matrix [18,19]. Indeed, several photomechanical composites, in which photomechanical crystals are integrated into polymer matrices, have been developed to date [20–29].

N-3,5-di-*tert*-butylsalicylide-3-nitroaniline (enol-**1**, Scheme 1) is a salicylideneaniline derivative that undergoes enol to *trans*-keto photoisomerization in the solid state and its thin crystals bend reversibly away from the light source upon ultraviolet (UV) exposure, based on photoisomerization [14,16]. We have previously reported that composite films in which enol-**1** crystals prepared by recrystallization from solutions are hybridized in polymer matrices exhibit similar bending by UV light [29]. In that study [29], however, the size of the hybridized enol-**1** crystals was not measured or optimized in detail. Given that enol-**1** crystals with a thickness of less than 40 μm exhibit significant bending, and those with a thickness of ~14 μm exhibit the most significant deformation based on Timoshenko's bimetal model [16], composite films incorporating enol-**1** crystals with a thickness of ~14 μm are also expected to bend significantly. Yet, it is challenging to prepare enough crystals of the desired uniform size simultaneously by recrystallization from solutions. Furthermore, in the previous work [29], mechanical properties of composite films, such as Young's modulus, were not measured and how their mechanical properties affect the photomechanical bending was unknown. In this work, we prepared thin, uniform enol-**1** microcrystals with a thickness of ~14 μm by using the reprecipitation method for the first time [30,31]. The mechanical properties of the composite films were measured by tensile testing, revealing the relationship between their mechanical properties and bending performance. We also focused on another salicylideneaniline derivative: *N*-3,5-di-*tert*-butylsalicylide-3-nitroaniline [15] (enol-**2**, Scheme 1). Enol-**2** crystals thinner than 10 μm show significant bending by photoisomerization, and those with a thickness of ~7 μm exhibit the most significant deformation based on Timoshenko's bimetal model [15]. We successfully fabricated light-driven crystal–polymer composite films in which thin (~7 μm) enol-**2** crystals are hybridized in a polymer matrix.

2. Results & discussion

2.1. Crystal preparation

Enol-**1** was synthesized by condensing 3,5-di-*tert*-butylsalicylaldehyde and 3-nitroaniline according to the method described in a previous report [16]. Enol-**1** microcrystals used for the hybridization were grown from enol-**1** nanocrystals as seed crystals. Firstly, enol-**1** nanocrystals were prepared using the reprecipitation method [30,31], i.e. by dispersing a methanol solution of enol-**1** into vigorously stirred water (Fig. 1a). Fig. 1b shows the time dependence of the average diameters of nanocrystals measured by the dynamic light scattering (DLS) method.

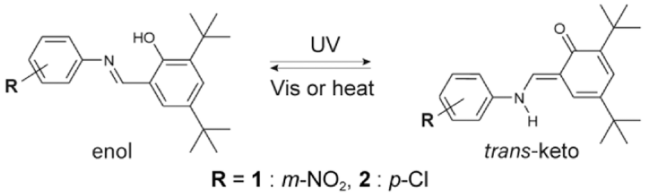

Scheme 1. Enol–*trans*-keto photoisomerization of **1** and **2**.

Two minutes after the methanol solution was dispersed into water, nanocrystals with a diameter of ~230 nm were formed, and the crystal size remained unchanged until 120 min. Fig. 1c displays the size distribution of enol-**1** nanocrystals at 20 min; the sizes fall in the range of 50–800 nm with an average value of 296 nm. The scanning electron microscopy (SEM) photographs of enol-**1** nanocrystals are depicted in Fig. 1d.

Enol-**1** seed nanocrystals dispersed in water were dropped into a saturated methanol solution of enol-**1** and left for two hours (Fig. 1e). Unlike simple recrystallization from solution, thin microcrystals with a uniform size and shape grew rapidly from the surface of the nanocrystals (Fig. 1 f). Fig. 1 g summarizes the size distribution of 80 randomly selected enol-**1** microcrystals. The length, width, and thickness were 344.1 ± 219.8, 25.7 ± 14.1, and 11.8 ± 7.0 μm (mean ± standard deviation, n = 80), respectively. Using the reprecipitation method, hundreds of single enol-**1** microcrystals with thicknesses of ~14 μm were obtained, which are expected to exhibit significant bending by photoisomerization [16].

2.2. Photomechanical bending of PDMS composite films

Composite films were then prepared in which enol-**1** single microcrystals prepared using the reprecipitation method were aligned in a polymer film (Fig. 2a, see the Experimental section for the detailed procedure). Among several candidate polymers (Table S1), polydimethylpolysiloxane (PDMS, molar ratio of vinyl terminated polydimethylsiloxane (500 g mol^{-1}) and 4–6 % (Mercaptopropyl) methylsiloxane]-dimethyl-siloxane copolymer (6000–8000 g mol^{-1}) = 1: 1, Fig. S1) and TB3031J (acrylic resin, ThreeBond Co., Ltd., Tokyo, Japan) were selected as candidate polymers on the basis that they satisfy the following requirements: (1) the precursor is commercially available; (2) the polymer is easily curable; (3) the enol-**1** crystal is insoluble in the precursors; and (4) the polymer is flexible and not brittle.

Upon 365-nm UV irradiation to an enol-**1**–PDMS composite film (length: 19.6 mm, width: 4.93 mm, thickness: 0.30 mm, crystal concentration: 5 wt% Fig. 2b, c) from the left side for 60 s, it bent away from the incident light and reached a maximum bending angle of 3.7° (Fig. 2d, e, Movie S1). The color of the film changed from yellow to orange because of photoisomerization of enol-**1** to *trans*-keto-**1** [14,16] (Fig. 2d). The maximum top surface temperature of the film increased from 23.9 to 38.6°C (ΔT = 14.7°C) by the photothermal effect (Fig. 2e). Immediately after the UV light was turned off, the film was then illuminated with 520-nm visible light and reverted to its original shape (Fig. 2d, e). This bending is attributed to the expansion of the irradiated left side, which is induced by photoisomerization of enol-**1** crystals, as previously reported (Fig. 2f) [29]. Indeed, the irradiated top face extended by 0.79 % (Fig. S5a). To confirm that this bending originates from photoisomerization rather than from the photothermal effect, the bending of another enol-**1**–PDMS film (length: 20.8 mm, width: 5.19 mm, thickness: 0.42 mm, crystal concentration: 5 wt%) upon 365-nm UV irradiation and subsequent 520-nm visible light irradiation with different visible light intensities (0, 38.0, 63.8 mW cm^{-2}) were measured (Fig. 2i, j). As the visible light intensity decreased, the speed of return after UV irradiation became slower (Fig. 2i) while the time profile of the top surface temperature showed no significant changes (Fig. 2j). These results indicate that photoisomerization is responsible for the bending of the enol-**1**–PDMS composite films. We also examined the bending behavior of a PDMS film that does not contain enol-**1** crystals. Upon UV irradiation to the PDMS film without enol-**1** crystals (length: 20.1 mm, width: 5.18 mm, thickness: 0.48 mm), it bent 0.21° away from the illumination direction, accompanied by an increase in the top surface temperature from 24.4 to 31.5°C (ΔT = 7.1°C) due to the photothermal effect of PDMS (Fig. 2g). This smaller bending angle of 0.21° compared to those of other composite films (> 1°) indicates that incorporation of enol-**1** microcrystals into the polymers are essential to generate significant bending behavior.

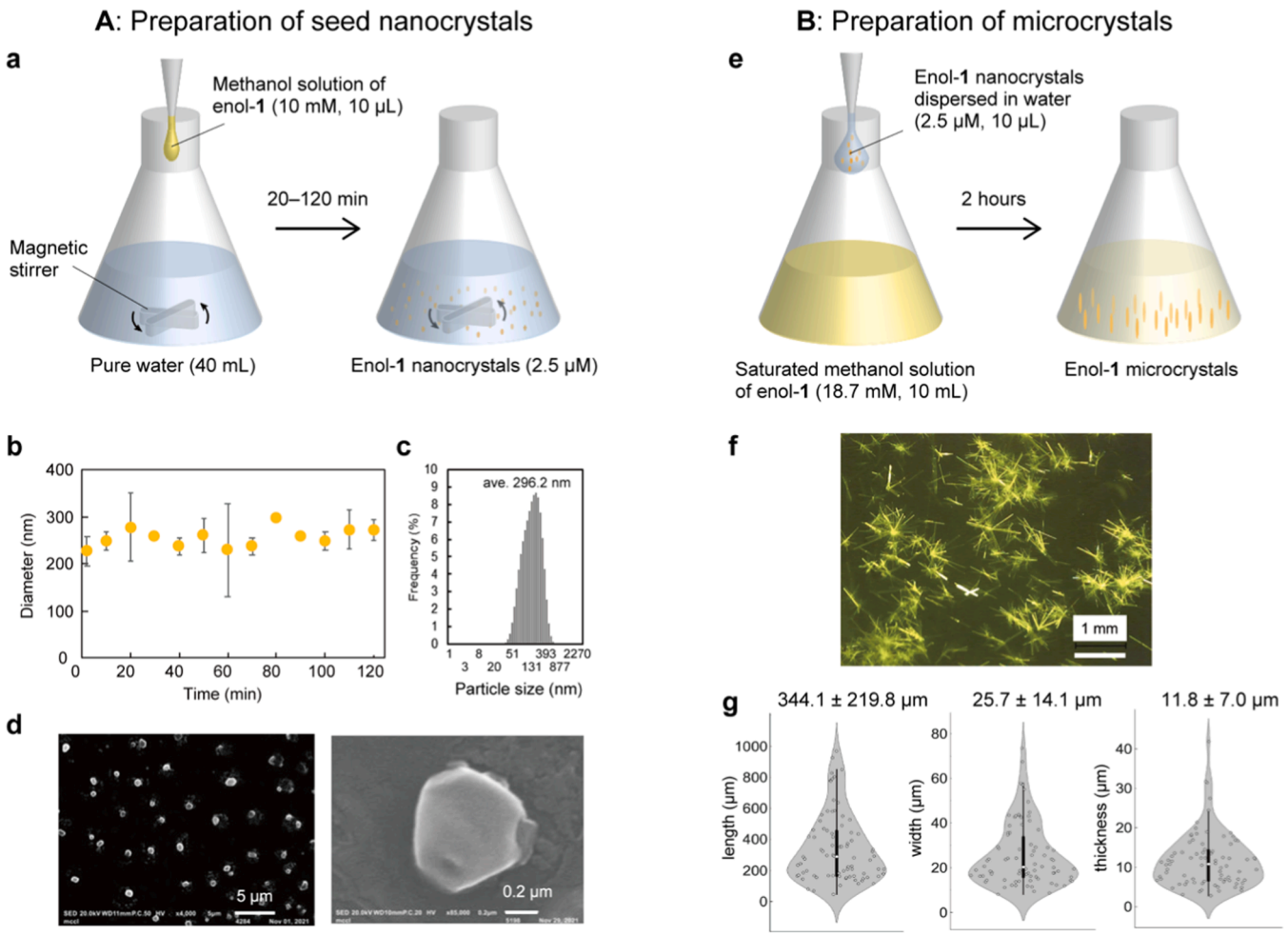

Fig. 1. (A: a–d) Preparation of enol-**1** nanocrystals by using the reprecipitation method. (a) Schematic illustration of crystal preparation. (b, c) Relationship between the time after dropping the methanol solution of enol-**1** to water and the average diameter of enol-**1** nanocrystals (n = 3) (b) and size distribution of enol-**1** nanocrystals at 20 min measured by the dynamic light scattering (DLS) method (c). (d) Scanning electron microscope (SEM) images of enol-**1** nanocrystals. (B: e–i) Preparation of enol-**1** microcrystals grown from enol-**1** nanocrystals as seed crystals, prepared using the reprecipitation method. (e) Schematic illustration of crystal preparation. (f) Photograph of enol-**1** microcrystals two hours after dropping enol-**1** nanocrystals. (g) Size distribution of 80 pieces of microcrystals. Mean ± standard deviation.

We also investigated enol-**1** concentration dependence of the bending angle and maximum top surface temperature (Fig. 2h, Fig. S2, S3). As for the bending angle, it increased as the enol-**1** concentration grew and showed the largest bending angle at 5 wt% but then decreased to reach 0.45° at 15 wt% (black solid circles in Fig. 2h). The maximum top surface temperature, on the other hand, inclined as the concentration increased from 0 to 3 wt% and then maintained the constant value between 36–45°C (orange open triangles, Fig. 2h). Still, no linear correlation was observed between the maximum bending angle and the top surface temperature. This result indicates that the bending of enol-**1**–PDMS composite films originates from photoisomerization of enol-**1** rather than from the photothermal effect since photothermal bending increased proportionally to the maximum top surface temperature [15]. The plausible reason that the composite film displayed the most significant deformation at 5 wt% can be because enol-**1** crystals were tightly packed and the crystals overlap each other in the composite film with a concentration of 7 wt% or higher, which can inhibit their movement through photoisomerization with each other, and thus the movement of crystals was not efficiently transmitted throughout the entire composite film. Note that the composite with the concentration of 3 wt% showed the fastest bending speed, followed by the composite with the concentration of 5 wt% (Fig. S4). The bending angles of the resulting composite films (< 4°) were still smaller than those of single enol-**1** crystals (> 10°) [16]. This is thought to be because the weight of the polymer acts as a force on the crystals, inhibiting the photomechanical bending of enol-**1** crystals to some extent. The bending of the composite film was reversible. Upon alternate irradiation of UV and visible light, the film repeated its bending and straightening motions for 500 cycles (750 min), but the film did not restore its original shape and the bending angle gradually declined after repeated bending and straightening (Fig. S6).

2.3. *Photomechanical bending of TB3031J composite films*

Next, the bending of an enol-**1**–TB3031J film was observed. Upon 365-nm light irradiation to an enol-**1**–TB3031J film (length: 18.7 mm, width: 5.44 mm, thickness: 0.28 mm, crystal concentration: 2.8 wt%, Fig. 3a, b) from the left side, the composite bent away from the illumination direction and reached a maximum bending angle of 14.2° in 60 s; the irradiated face extended by 1.23 % during bending (Fig. S5b). The maximum top surface temperature increased from 22.0 to 52.8°C (ΔT = 30.8°C) owing to the photothermal effect (Fig. 3c, d, Movie S2). Immediately after turning off the UV light and turning on 520-nm visible light, it bent 1.9° toward the illumination direction in 20 s but did not restore its original shape even after 60 s of visible light irradiation (Fig. 3c, d). A similar trend was observed for other enol-**1**–TB3031J films of a similar size that contained 3.5 and 4.7 wt% crystals (Fig. S7).

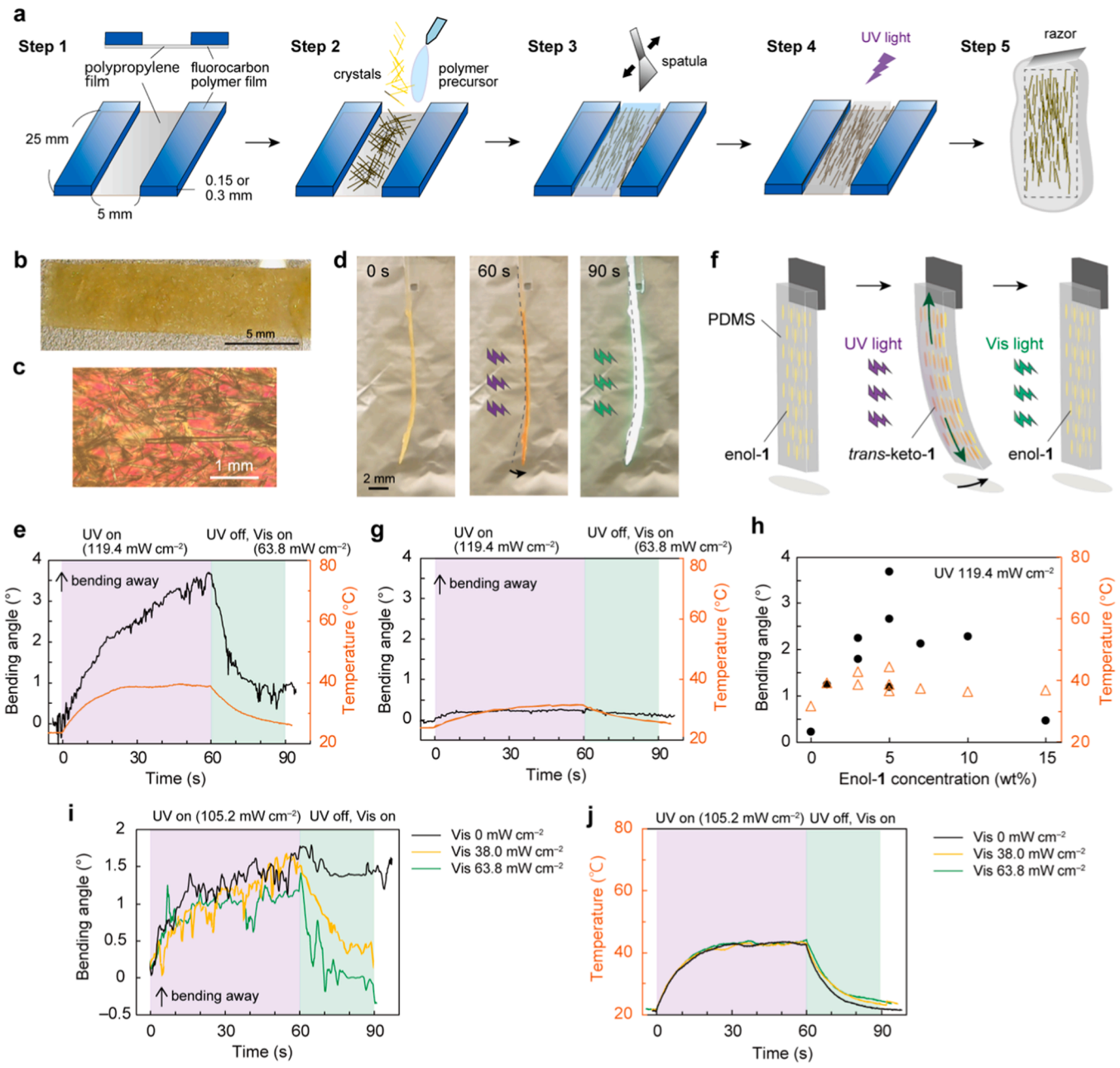

Fig. 2. Bending of enol-**1**–PDMS composite films. (a) Schematic illustration of preparation of composite films. (b) Photograph of the film from the top and (c) its enlarged polarized microscopic image. (d) Sequential snapshots of bending before UV irradiation (left), after UV irradiation for 60 s (center), and upon visible light irradiation for 30 s (right). (e) Time dependence of the bending angle (black) and top surface temperature (orange). (f) Schematic illustration of the bending mechanism through photoisomerization from enol-**1** to *trans*-keto-**1**. (g) Time dependence of the bending angle (black) and top surface temperature (orange) of a PDMS film without enol-**1** crystals upon UV irradiation for 60 s and subsequent visible light irradiation for 30 s. (h) Enol-**1** concentration dependence of the maximum bending angle (black solid circles) and maximum irradiated surface temperature (orange open triangles). (i, j) Time dependence of the bending angle (i) and the top surface temperature (j) of a composite film upon UV irradiation and subsequent visible light irradiation with different intensities.

We then observed the bending of a TB3031J film without enol-**1** (length: 17.6 mm, width: 5.60 mm, thickness: 0.18 mm). Upon UV irradiation for 60 s, it bent 5.5° away with a top surface temperature increase from 22.6 to 31.0°C ($\Delta T = 8.4$°C). After UV irradiation and subsequent visible light illumination, the top surface temperature returned to the initial temperature, but the film did not revert to its original shape. Rather, it bent further away from the illumination direction, reaching a maximum bending angle of 6.6° in 60 s (Fig. 3f). We hypothesized that the bending was caused by the expansion of the irradiated left face by the photothermal effect rather than by photoisomerization (Fig. 3e). Indeed, a TB3031J film elongated upon heating on a hot plate, exhibiting a positive thermal expansion coefficient of 5.0×10^{-5} °C^{-1} (Fig. 3g).

To confirm that the bending of enol-**1**–TB3031J composites originates from the photothermal effect, we prepared a TB3031J composite film that incorporated another enol-**2** microcrystals (Scheme 1) [15]. Enol-**2** is a salicylideneaniline derivative that exhibits a similar absorption spectrum to enol-**1**, but thin enol-**2** single crystals alone bend toward the illumination direction upon UV irradiation [15], which is the opposite of enol-**1**. Microcrystals of enol-**2** thinner than 10 μm exhibit significant bending through photoisomerization, and those with a thickness of ~7 μm exhibit the most significant deformation based on

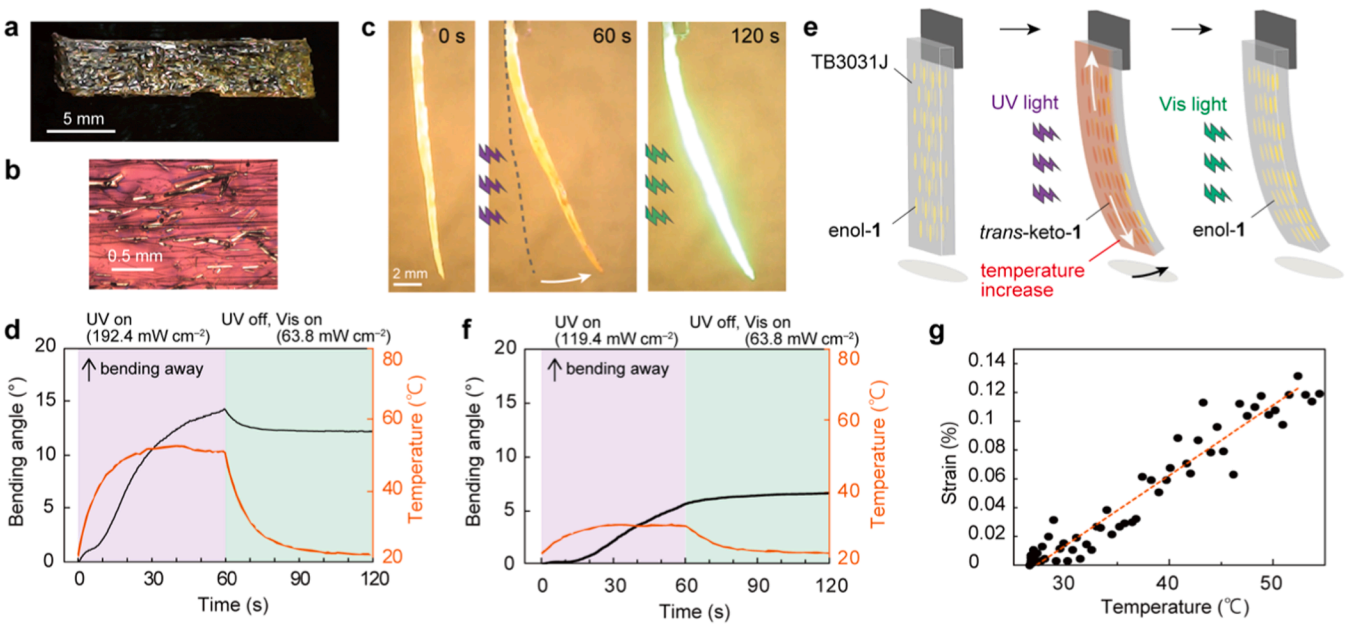

Fig. 3. Bending of the enol-**1**–TB3031J composite films. (a) Photograph of the film from the top and (b) its enlarged polarized microscopic image. (c) Sequential snapshots of bending before UV irradiation (left), after UV irradiation for 60 s (center), and upon visible light irradiation for 60 s (right). (d) Time dependence of the bending angle (black) and top surface temperature (orange). (e) Schematic illustration of the bending mechanism through the photothermal effect. (f) Time dependence of the bending angle (black) and the top surface temperature (orange) of a TB3031J film without enol-**1** crystals upon UV irradiation for 60 s and subsequent visible light irradiation for 60 s. (g) Temperature dependence of the thermal strain of a TB3031J film upon heating from 25 to 55°C.

Timoshenko's bimetal model [15]. We attempted to prepare thin enol-**2** microcrystals (~7 μm) by the reprecipitation method, but the obtained crystals were thicker than 15 μm (Fig. S8). We then prepared enol-**2** crystals by sublimation. Powder enol-**2** crystals were mounted in a glass dish, covered with a glass lid, and heated at 220 °C for 2 h, yielding thin crystals with a thickness of 8.8 ± 4.2 μm (mean ± standard deviation, n = 40, Fig. S9). Enol-**2**–TB3031J composite films were then fabricated by incorporating these thin enol-**2** microcrystals prepared by sublimation.

Under 365-nm UV illumination to an enol-**2**–TB3031J film (length: 18.9 mm, width: 5.72 mm, thickness: 0.16 mm, crystal concentration: 2.6 wt%, Fig. 4a, b), the film bent 16.8° away from the light source in 60 s accompanied by an increase in the temperature of the top surface from 21.6 to 48.0°C (ΔT = 26.4°C) by the photothermal effect (Fig. 4c, d, Movie S3). The irradiated top surface extended by 1.18 % during bending (Fig. S5c). Upon cessation of UV irradiation and 520-nm visible light irradiation, the top surface temperature decreased to 22.8°C in 60 s but the film did not restore its original shape (Fig. 4c, d), in a manner similar to that observed for enol-**1**–TB3031J films. Other enol-**2**–TB3031J films also displayed a similar irreversible bending motion away from UV light (Fig. S10). If the composite film were driven by photoisomerization, the irradiated top surface contracts because of photoisomerization of enol-**2** and the bending direction of the composite film should have been the same as that of the single crystal, bending toward the light [28]; however, in fact, its top surface extended by 1.18 % (Fig. S5c) and it bent away from the light. Therefore, the bending of TB3031J composite films originates from the photothermal effect of the polymer matrix rather than from photoisomerization of microcrystals.

2.4. Mechanical properties of composite films

The mechanical properties of composite films were measured in order to explain the reversibility of the bending of PDMS composite films and the irreversibility of the bending of TB3031J composite films. Fig. 5 shows the stress–strain curves of the polymer and composite films obtained through uniaxial elongation of the tensile testing, as well as those of enol-**1** single crystals obtained through cantilever bending tests. The Young's modulus, strain and stress are summarized in Table 1. Enol-**1** crystals displayed a linear relationship between stress and strain over a strain range of up to 0.939 ± 0.071 % (mean ± standard error, Fig. 5a, Fig. S12), indicating that enol-**1** crystals are elastic at that region. The Young's modulus, calculated from the slope of the stress–strain curve, was determined to be 2.210 ± 0.254 GPa (mean ± standard error), which is comparable to other organic crystals [17]. Fig. 5b and Fig. S13a show the stress–strain curves of PDMS films; they exhibited a linear relationship between stress and strain over a strain range of strains up to 41.8 ± 7.7 % and the Young's modulus was calculated to be 0.0498 ± 0.0014 MPa. Enol-**1**–PDMS composite films also displayed elastic deformation over a strain range of up to 29.9 ± 1.2 %, with a Young's modulus of 0.0943 ± 0.0046 MPa (Fig. 5c, Fig. S13b). These results show that PDMS and composite films exhibit elastic deformation for strains that are more than one order of magnitude greater than those of enol-**1**, while the Young's modulus is four orders of magnitude lower. The reason that the composite film exhibited mechanical properties similar to PDMS rather than enol-**1** would be because of the low concentration of enol-**1** (5 wt%).

Fig. 5d and Fig. S14a show the stress–strain curves of TB3031J films. Unlike PDMS films and PDMS–enol-**1** composite films, the stress–strain curves of TB3031J films exhibited nonlinear correlations. In one sample, the slope between strain and stress decreased continuously as strain increased (see sample 1 in Fig. S14a). In another sample, the slope initially increased with increasing strain, before beginning to decrease and follow an S-shaped curve (see sample 9 in Fig. S14a). The strain at the elastic limit—the maximum strain value within the range where the stress–strain curve can be linearly approximated ($R^2 \geq 0.99$)—was 2.18 ± 0.003 %, one order of magnitude smaller than that of PDMS films (see the red lines in Fig. S14b). Enol-**1**–TB3031J composite films showed similar mechanical properties, with a strain at the elastic limit of 4.81 ± 0.68 % (Fig. 5e, Fig. S14b). Owing to their lower elasticity, enol-**1**–TB3031J composite films were not expected to return to their original straight shape after turning off UV light. However, note that when the UV light irradiation time was shortened from 60 to 10 s, enol-**1**–TB3031J films exhibited reversible bending at least 20 times

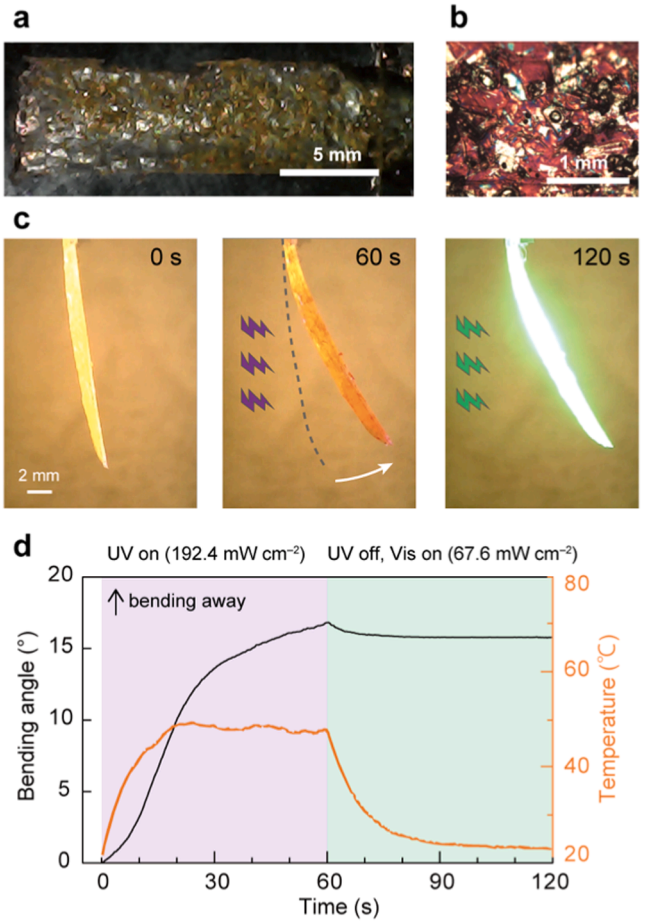

Fig. 4. Bending of an enol-**2**–TB3031J composite film. (a) Photograph of the film from the top and (b) its enlarged polarized microscopic image. (c) Sequential snapshots of bending before UV irradiation (left), after UV irradiation for 60 s (center), and upon visible light irradiation for 60 s (right). (d) Time dependence of the bending angle (black) and maximum top surface temperature (orange).

(Fig. S11), because the maximum bending angle of the enol-**1**–TB3031J films decreased and, consequently, the maximum strain they undergo was reduced. The Young's moduli of TB3031J alone and enol-**1**–TB3031J composite films were 127 ± 23.2 MPa and 110 ± 11.5 MPa, respectively, three orders of magnitude higher than those of PDMS (Table 1). This higher Young's modulus of TB3031J compared to that of PDMS could be responsible for the negligible bending arising from photoisomerization of enol-**1** crystals, because when the Young's modulus increases by three orders of magnitude, a stress three orders of magnitude greater is necessary to generate the same strain.

3. Conclusion

In summary, centimeter-scale light-responsive crystal–polymer composite film actuators were developed. Microcrystals of *N*-3,5-di-*tert*-butylsalicylide-3-nitroaniline (enol-**1**) with a thickness of ~14 μm were grown from enol-**1** nanocrystals as seed crystals prepared by the reprecipitation method. Two types of composite photoactuator were fabricated by aligning enol-**1** microcrystals into two commercially available polymers, namely, PDMS and TB3031J (acrylic resin). Upon 365-nm UV light irradiation to enol-**1**–PDMS composite films, they bent away from the light source through photoisomerization of enol-**1** crystals to *trans*-keto-**1** and then returned to the original shape following 520-nm visible light irradiation through back isomerization from *trans*-keto to enol. The film exhibited the most significant deformation when the concentration of enol-**1** microcrystals is 5 wt%. Enol-**1**–TB3031J composite films bent away from UV light through the photothermal effect, but they did not revert to the unbent shape after UV irradiation. Tensile testing of the polymer and composite films disclosed that the PDMS films were elastic and could withstand strain of over 25 %, whereas the TB3031J films underwent plastic deformation. The lower elasticity of TB3031J results in the irreversible bending of enol-**1**–TB3031J composite films. Furthermore, we have fabricated enol-**2**–TB3031J composite films, in which microcrystals of *N*-3,5-di-*tert*-butylsalicylide-4-chloroaniline (enol-**2**) prepared by sublimation were aligned in TB3031J. Upon UV irradiation they bend away from the light source through the photothermal effect. This work demonstrates that polymers with higher elasticity are preferable for fabricating of composite actuators that exhibit enhanced repeatability. The composite fabrication method demonstrated in this study could also be applied to the preparation of composites containing other organic photomechanical organic crystals, such as diarylethene and azobenzene. Overall, this work provides insight into the development of light-responsive crystal–polymer composite actuators that are larger in size (centimeter scale) and easier to process, which are formidable challenges for photomechanical crystals alone. The actuation performance of PDMS and TB3031J composites, including the bending angle, response time, and bending repeatability, was comparable to that of previously reported light-responsive crystal–polymer composites (see Table S2). To facilitate their practical implementation in actuators and soft robots, future research must address the development of composites with enhanced actuation performance (e.g. higher levels of repeatability over 10,000 cycles).

4. Methods

4.1. Preparation of single enol-1 microcrystals using the reprecipitation method

10 μL of methanol solution of enol-**1** (concentration: 10 mM) was dispersed dropwise into 40 mL of water vigorously stirred in a conical flask and stirring was continued for several minutes to prepare nanocrystals of enol-**1** dispersed in water (concentration: 2.5 μM). Then 10 μL of water in which enol-**1** nanocrystals were dispersed was dropped into 10 mL of saturated methanol solution of enol-**1** (concentration: 18.7 mM) in a conical flask. The methanol solution was left for two hours without stirring to produce enol-**1** microcrystals. All experiments were conducted at room temperature under atmosphere pressure.

4.2. Dynamic light scattering and scanning electron microscopy measurements

Dynamic light scattering (DLS) measurements were conducted using a dynamic light scattering particle size analyzer (DLSPSA, LB-550, HORIBA, Ltd., Kyoto, Japan). The scanning electron microscopy (SEM) measurements were conducted using a compact SEM (IT-100LA, JEOL Ltd., Tokyo, Japan). A small amount of the particle dispersion of nanocrystals was dropped onto a cover glass, dried, and used to create a sample for measurement. The sample was then coated with platinum twice using a sputter from different directions.

4.3. Preparation of crystal–polymer composite films

Composite films were fabricated using a mold (25 mm × 5 mm × 0.15 or 0.30 mm) made of commercially available polypropylene and fluorocarbon polymer films. A suspension of enol-**1** microcrystals in the polymer precursor was poured into the mold, and its surface was gently rubbed with a spatula several times along the length direction of the mold to align the microcrystals. The suspension was then cured for several minutes using UV light (365 nm, UV-1H, Kantum Ushikata Co., Ltd., Yokohama, Japan). The suspension was irradiated firstly from the

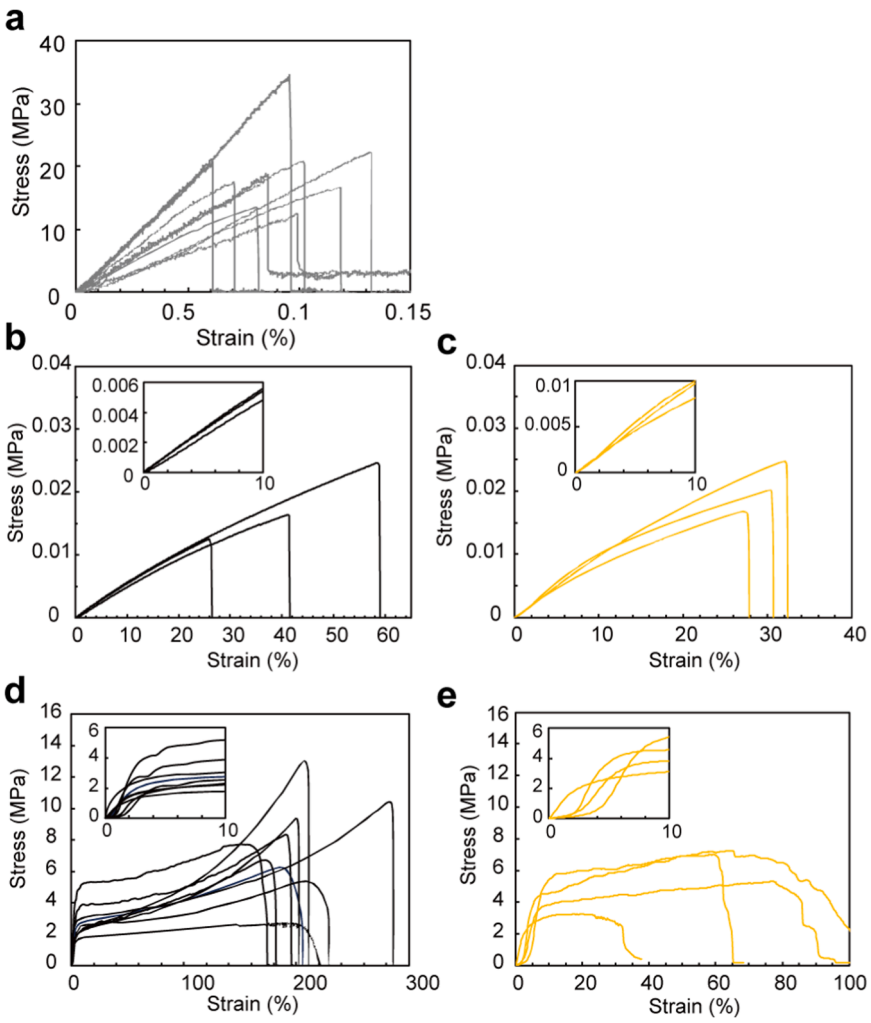

Fig. 5. Stress–strain curves of enol-**1** single crystals (a), PDMS films (b), enol-**1**–PDMS films (enol-**1** concentration: 5 wt%) (c), TB3031J films (d), and enol-**1**–TB3031J films (enol-**1** concentration: 2.8–4 %) (e). Inset in (b)–(e): enlarged stress–strain curves over a range of strains up to 10 %.

Table 1
Summary of Young's modulus, strain and stress of enol-**1** crystals, polymers, and composite films. Mean ± standard error.

Name	n	Young's modulus [MPa]	Strain at elastic limit [%]	Stress at elastic limit [MPa]
Enol-**1**	9	2210 ± 254	0.939 ± 0.071	19.8 ± 2.0
PDMS	3	0.0498 ± 0.0014	41.8 ± 7.7	0.0178 ± 0.0029
Enol-**1**–PDMS	3	0.0943 ± 0.0046	29.9 ± 1.2	0.0206 ± 0.0019
TB3031J	9	127 ± 23.2	2.18 ± 0.003	1.69 ± 0.19
Enol-**1**–TB3031J	4	110 ± 11.5	4.81 ± 0.68	2.97 ± 0.24

bottom side of the mold and then from the top side. This is because if the UV light irradiation is initially applied from the top, the air bubbles in the suspension prior to curing lose their escape route and remain in the composite film. After curing, the edges of the composite film were trimmed with a razor to produce the rectangular composite film (Fig. 2a).

4.4. Tensile testing

Tensile testing was conducted using a universal material testing machine (RTG-1210, A&D Company, Limited, Tokyo, Japan) to measure mechanical properties, including Young's modulus and strain and stress at which the transition from elastic to plastic occurs. For polymer and composite films, both ends of a sample were cramped with a jaw (J-JFM-50N, A&D Company, Limited) and the sample was pulled upward at a speed of 1 mm/min to measure the relationship between the displacement and the load. For single enol-**1** crystals, Young's modulus was measured based on a cantilever bending test, as previously reported [32].

4.5. Observation of light-driven bending of crystal–polymer composite films

One end of a sample was fixed to a glass plate with a glue and a top face of the sample was irradiated with UV light (365 nm, UV-1H, Kantum Ushikata Co., Ltd.) and visible light (520 nm, PJ2–3005–4CA-PE, CCS Inc., Kyoto, Japan) to examine photomechanical bending. The irradiated top surface temperature was recorded with an infrared camera (FSV-2000, Apiste Corporation, Osaka, Japan). All experiments were conducted at room temperature under atmosphere pressure. Time dependence of the bending angle was analyzed using *Tracker* [33], a free video analysis and modeling tool.

CRediT authorship contribution statement

Yuki Hagiwara: Validation, Funding acquisition. **Taiki Goto:** Investigation. **Jérémy Odent:** Writing – review & editing, Supervision, Project administration. **Jean-Marie Raquez:** Project administration.

Shodai Hasebe: Writing – review & editing, Writing – original draft, Visualization, Validation, Funding acquisition. **Takashi Ueno:** Visualization, Investigation. **Hideko Koshima:** Writing – review & editing, Supervision, Funding acquisition, Conceptualization. **Toru Asahi:** Project administration.

Declaration of Competing Interest

The authors declare that they have no known competing financial interests or personal relationships that could have appeared to influence the work reported in this paper.

Acknowledgements

This research was supported by JSPS KAKENHI Grant number JP17H03107 for H.K., JP22KJ2958 for S.H. and JP22KJ2879 for Y.H., respectively, Iketani Science and Technology Foundation (0351227-A) for S.H., the Grant-in-Aid for Young Scientists (Early Bird) at Waseda Research Institute for Science and Engineering for S.H. and Y.H. T.U. is grateful to the staff in the University of Mons and Waseda University for the support of short-term staying in the University of Mons from 7 August 2022–1 October 2022. S.H. and Y.H. thank the Graduate Program for Power Energy Professionals (PEP), Waseda University from MEXT WISE Program.

Appendix A. Supporting information

Supplementary data associated with this article can be found in the online version at doi:10.1016/j.mtcomm.2025.114375.

Data availability

Data will be made available on request.

References

[1] H. Koshima. Mechanically Responsive Materials for Soft Robotics, Wiley-VCH, Weinheim, 2020.
[2] H. Zeng, P. Wasylczyk, D.S. Wiersma, A. Priimagi, Light robots: bridging the gap between microrobotics and photomechanics in soft materials, Adv. Mater. 30 (2018) 1703554.
[3] L. Qin, X. Liu, Y. Yu, Soft actuators of liquid crystal polymers fueled by light from ultraviolet to near infrared, Adv. Opt. Mater. 9 (2021) 2001743.
[4] Y. Yu, M. Nakano, T. Ikeda, Directed bending of a polymer film by light, Nature 425 (2003) 145.
[5] C. He, Y. Xiao, S. Wang, H. Lu, X. Li, L. Xu, C. Wang, Y. Tu, Main-chain azobenzene poly(etherester) multiblock copolymers for strong and tough light-driven actuators, ACS Appl. Mater. Interfaces 16 (2024) 56469–56480.
[6] J. Huang, H. Liao, Y. Zhang, W. Wu, M. Wu, X. Gong, Light-driven actuator using superhydrophobic polymer composite films for biomimetics and water-droplet manipulation, ACS Appl. Mater. Interfaces 17 (2025) 47743–47752.
[7] W.M. Awad, D.W. Davies, D. Kitagawa, J.M. Halabi, I. Tahir, F. Tong, G. Campillo-Alvarado, A.G. Shtukenberg, Y. Hagiwara, M. Almehairbi, L. Lan, S. Hasebe, D. P. Karothu, S. Mohamed, H. Koshima, S. Kobatake, Y. Diao, R. Chandrasekar, H. Zhang, C.C. Sun, C. Bardeen, R.O. Al-Kaysi, B. Kahr, P. Naumov, Mechanical properties and peculiarities of molecular crystals, Chem. Soc. Rev. 52 (2023) 3098–3169.
[8] S. Kobatake, S. Takami, H. Muto, T. Ishimawa, M. Irie, Rapid and reversible shape changes of molecular crystals on photoirradiation, Nature 446 (2007) 778–781.
[9] M. Irie, Diarylethene Molecular Photoswitches, Wiley-VCH: Weinheim, Germany, 2021.
[10] H. Koshima, N. Ojima, H. Uchimoto, Mechanical motion of azobenzene crystals upon photoirradiation, J. Am. Chem. Soc. 131 (2009) 6890–6891.
[11] T. Taniguchi, T. Asahi, H. Koshima, Photomechanical azobenzene crystals, crystals 9 (2019) 437.
[12] L. Zhu, R.O. Al-Kaysi, C.J. Bardeen, Reversible photoinduced twisting of molecular crystal microribbons, J. Am. Chem. Soc. 133 (2011) 12569–12575.
[13] F. Tong, C.J. Bardeen, R.O. Al-Kaysi, Photomechanical Crystals Made from Anthracene Derivatives, in: H. Koshima (Ed.), In Mechanically Responsive Materials for Soft Robotics, Wiley-VCH, Weinheim, Germany, 2020, pp. 29–56.
[14] H. Koshima, K. Takechi, H. Uchimoto, M. Shiro, D. Hashizume, Photomechanical bending of salicylideneaniline crystals, Chem. Commun. 47 (2011) 11423–11425.
[15] S. Hasebe, Y. Hagiwara, K. Hirata, T. Asahi, H. Koshima, Crystal actuation switching by crystal thickness and light wavelength, Mater. Adv. 3 (2022) 7098–7106.
[16] S. Hasebe, Y. Hagiwara, T. Ueno, T. Asahi, H. Koshima, Negative to positive axial thermal expansion switching of an organic crystal: contribution to multistep photoactuation, Chem. Sci. 15 (2024) 1088–1097.
[17] S. Hasebe, Y. Hagiwara, T. Asahi, H. Koshima, Actuation performance and versatility of photothermally driven organic crystals, Angew. Chem. Int. Ed. 64 (2025) e202418570.
[18] C. Altinkok, G. Acik, O. Daglar, H. Durmaz, I. Tunc, E. Agel, A facile approach for the fabrication of antibacterial nanocomposites: a case study for AgNWs/Poly(1,4-Cyclohexanedimethylene Acetylene Dicarboxylate) composite networks by aza-Michael addition, Eur. Polym. J. 169 (2022) 111130.
[19] S. Dong, X. Zhang, Y. Xiong, X. Mao, X. Wu, N. Li, S. Yang, H. Hua, Antimicrobial thin-film composite polyamide nanofiltration membrane with high desalination and flux performance manufactured through a novel UV light driven photoreduction method that generates dispersed silver nanoparticles" *Desalin*, Water Treat. 282 (2023) 10–22.
[20] T. Lan, W. Chen, Hybrid nanoscale organic molecular crystals assembly as a photon-controlled actuator, Angew. Chem. Int. Ed. 52 (2013) 6496–6500.
[21] S.C. Sahoo, N.K. Nath, L. Zhang, M.H. Semreen, T.H. Al-Tel, P. Naumov, RSC Adv. 4 (2014) 7640–7647.
[22] Q. Yu, X. Yang, Y. Chen, K. Yu, J. Gao, Z. Liu, P. Cheng, Z. Zhang, B. Aguila, S. Ma, Fabrication of light-triggered soft artificial muscles via a mixed-matrix membrane strategy, Angew. Chem. Int. Ed. 57 (2018) 10192–10196.
[23] Y.-X. Shi, W.-H. Zhang, B.F. Abrahams, P. Braunstein, J.-P. Lang, Fabrication of photoactuators: macroscopic photomechanical responses of metal–organic frameworks to irradiation by UV light, Angew. Chem. Int. Ed. 58 (2019) 9453–9458.
[24] P. Xu, Q. Yu, Y. Chen, P. Cheng, Z. Zhang, Protective coating with crystalline shells to fabricate dual-stimuli responsive actuators, CCS Chem. 4 (2022) 205–213.
[25] M. Singh, V.G. Abhijitha, B.R.K. Nanda, D. Pareek, S. Nath, S. Anwar, A. Kumar, P. K. Nanda, S.C. Sahoo, Excellent photo actuation in crystal-polymer composite by transfer of mechanical energy, Chem. Eng. J. 464 (2023) 142665.
[26] Y. Wei, K. Chen, S. Zhu, W. Wu, H. Zhao, X. Huang, N. Wang, L. Zhou, T. Wang, J. Wang, H. Hao, Photoactuators based on plastically flexible α-cyanostilbene molecular crystals driven by the solid-state [2+2] cycloaddition reaction, small 20 (2023) 2307756.
[27] W. Xu, D.M. Sanchez, U. Raucci, H. Zhou, X. Dong, M. Hu, C.J. Bardeen, T. J. Martinez, R.C. Hayward, Photo-actuators via epitaxial growth of microcrystal arrays in polymer membranes, Nat. Mater. 22 (2023) 1152–1159.
[28] H. Koshima, M. Matsudomi, Y. Uemura, F. Kimura, T. Kimura, Light-driven bending of polymer films in which salicylidenephenylethylamine crystals are aligned magnetically, Chem. Lett. 42 (2013) 1517–1519.
[29] S. Hasebe, D. Matsuura, T. Mizukawa, T. Asahi, H. Koshima, Light-driven crystal–polymer hybrid actuators, Front. Robot. AI 8 (2021) 684287.
[30] H. Kasai, H.S. Nalwa, H. Oikawa, S. Okada, H. Matsuda, N. Minami, A. Kakuta, K. Ono, A. Mukoh, H. Nakanishi, A novel preparation method of organic microcrystals, Jpn. J. Appl. Phys. 31 (1992). L1132.
[31] H. Nakanishi, H. Oikawa, in: H. Masuhara, H. Nakanishi, K. Sasaki (Eds.), Reprecipitation Method for Organic Nanocrystals, Single Organic Nanoparticles, Springer, Berlin, 2003, pp. 17–31.
[32] Y. Hagiwara, S. Hasebe, H. Fujisawa, J. Morikawa, T. Asahi, H. Koshima, Photothermally induced natural vibration for versatile and high-speed actuation of crystals, Nat. Commun. 14 (2023) 1354.
[33] D. Brown, W. Christian, R.M. Hanson, 2025, Tracker Video Analysis and Modeling Tool, ver. 6.3.0⟨https://opensourcephysics.github.io/tracker-website/⟩.